OPEN ACCESS
IOP Publishing
Superconductor Science and Technology
Supercond. Sci. Technol. 33 (2020) 044009 (12pp)
https://doi.org/10.1088/1361-6668/ab6dc2

Distribution of the superconducting critical current density within a Gd–Ba–Cu–O single grain

Yunhua Shi[1], Michael Gough, Anthony R Dennis, John H Durrell and David A Cardwell

Department of Engineering, University of Cambridge, Trumpington Street, Cambridge CB2 1PZ, United Kingdom

E-mail: ys206@cam.ac.uk

Received 11 October 2019, revised 24 December 2019
Accepted for publication 20 January 2020
Published 20 February 2020

Abstract

The magnitude of the maximum trapped magnetic field in a bulk, single-grain superconductor is a key performance figure of merit. This is determined, generally, by the magnitude of the critical current density, J_c, and the length scale over which it flows. As with all type-II superconductors, J_c is related closely to the microstructure of the superconducting material and, in the case of RE–Ba–Cu–O [(RE)BCO, where RE is a rare-earth element or yttrium] single grains, RE_2BaCuO_5 (RE-211) inclusions in the superconducting $REBa_2Cu_3O_{7-\delta}$ (RE-123) phase matrix are key microstructural features that act effectively as flux pinning centres. Although the distribution of RE-211 in single-grain bulk superconductors has been studied extensively, the variation of J_c within a given sample has been much investigated much less thoroughly. A detailed experimental understanding of the variation of J_c in these technologically important materials, therefore, is required given the growing popularity and significance of numerical techniques for modelling the behaviour of type-II bulk superconductors. Here we report a systematic investigation of the correlation between Gd-211 particle density and sample porosity, which are microstructural features, and T_c and J_c in a Gd–Ba–Cu–O bulk, single grain fabricated using a buffer layer and a supply of additional liquid phase. This was performed by cutting the sample into numerous sub-specimens of approximate dimensions $1.8 \times 2.8 \times 1.5\,mm^3$. We observe that J_c decreases with distance from the seed, although more strongly with distance along the *c*-axis than along the *a–b* plane. In contrast to what might be expected given the assumed contribution of RE-211 inclusions to flux pinning, we find no evidence of a clear correlation between the local RE-211 precipitate density and local critical current on a length scale of mm. We observe that the porosity of the sample is a more dominant factor in determining the distribution of J_c within a single grain.

Keywords: GdBCO single grain, distribution of J_c, porosity, microstructure, Gd-211, buffer technique

(Some figures may appear in colour only in the online journal)

Introduction

The presence of grain boundaries in RE–Ba–Cu–O [(RE)BCO, where RE is a rare-earth element or yttrium] bulk superconductors, misoriented by more than a few degrees, limits significantly the macroscopic superconducting properties of these potentially technologically important materials [1,2]. As a

[1] Author to whom any correspondence should be addressed.

result, bulk (RE)BCO superconductors suitable for practical applications have to be fabricated in the form of large, single grains with uniform superconducting properties throughout the sample microstructure. Unfortunately, however, the critical current density, J_c, in these materials is observed to vary significantly both within a single grain and between single grains notionally fabricated by the same melt processing technique. This variation is intrinsic to the melt growth process employed and to the ceramic-like nature of these materials, which typically contain microcracks within the sample microstructure. The ability of bulk superconductors to generate trapped magnetic field depends directly on the critical current density, although mechanical weakness in the sample microstructure may result in their premature failure under the action of Lorentz forces in the presence of large applied magnetic fields. Critical current density, however, depends on a wide variety of factors ranging from the effectiveness and density of pinning centres on the length scale of the vortex core to material defects and grain boundaries, porosity and cracks at the mesoscopic scale.

Bulk superconductors consist typically of a single grain, fabricated usually by a melt process, which is composed of a continuous superconducting (RE)$Ba_2Cu_3O_{7-\delta}$ phase matrix (RE-123—where RE = Nd, Sm, Gd, Dy, and Y or combined RE element) with embedded, discrete RE_2BaCuO_5 precipitates (RE-211) that act as effective flux pinning sites. Most studies of these materials report typically only a single J_c-B curve obtained from one specimen at one position within a given sample, which contains relatively little useful information about the applied potential of the complete single grain. In addition, reported $J_c(B = 0)$ values in Y–Ba–Cu–O single grains can vary from 2×10^4 to 2×10^5 A cm^{-2} at 77 K [3–7]. Dewhurst *et al* reported the distribution of J_c across the entire cross-section of a YBCO single grain [6]. One of the conclusions of this investigation was that J_c of the sample in the region directly below and adjacent to the Sm seed crystal exhibited a lower J_c by almost a factor of 3 relative to the surrounding material [6]. These authors postulated that this was due to Sm contamination from the seed crystal, which had the effect of locally reducing T_c [8]. This suggests that the distribution of the local J_c in bulk superconductors is not only affected critically by the sample microstructure, but also by any local variation in T_c. The development of the so-called buffer seeding technique [9–14] has helped to improve the reliability of the seeding process, and has ameliorated the problem of contamination from the seed reported in these early studies.

This paper reports the results of experiments aimed at obtaining a systematic understanding the distribution of local J_c in bulk (RE)BCO superconductors. This involves examination of the entire cross-section of a GdBCO single grain fabricated in air by the so-called top seeded melt-growth (TSMG) technique [15] using the buffer seed technique. The single grain sample was divided into many sub-specimens and the T_c and M–H characteristic of each sub-specimen measured at 77 K. The microstructure of each sub-specimen, including porosity and the size and distribution of Gd-211 particles, was analysed at positions within the parent single grain and correlated with the J_c measurements. The observed trends and range of fluctuations in local J_c of the GdBCO single grain are discussed in detail.

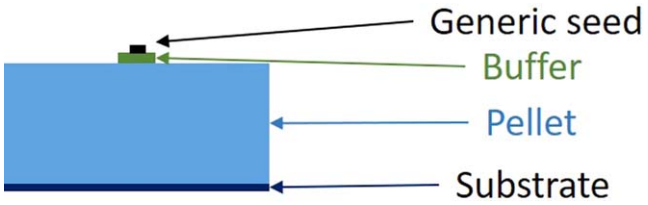

Figure 1. Schematic illustration of the precursor arrangement used for melt processing.

Experimental

Melt-processing

The raw powders of Gd-123 and Gd-211 were sourced from Toshima, 99.9% purity (grain size: Gd-123, 2–3 μm; Gd-211, 1–2 μm). The base Gd–Ba–Cu–O standard powders were of composition [75 wt% $GdBa_2Cu_3O_{7-\delta}$ (Gd-123) + 25 wt% Gd_2BaCuO_5 (Gd-211)] + 0.5 wt% CeO_2. The precursor powders were mixed thoroughly using an automatic pestle and mortar for 2 h and prior to pressing into a pellet of mass 20 g for melt processing using the arrangement shown schematically in figure 1. A generic seed [16] (of composition [(Nd123 + 0.12 Nd422)+1 wt%MgO]) was placed at the centre of the top surface of the assembly and a buffer [12,17] was inserted between the seed and the pellet. The composition of the buffer was 75 wt% Gd-123 + 25 wt% Gd-211 for the GdBCO sample. A liquid-rich phase substrate was used to prevent unwanted grain nucleation at the bottom of the sample, in addition to supplying liquid $Ba_3Cu_5O_8$ back to the pellet during melt growth [18,19].

The entire arrangement of the pellet, buffer, generic seed and substrate was placed in a box furnace, heated to 1080 °C at 70 °C h^{-1} and held for one hour. The arrangement was then cooled at 50°C/h to 1035 °C, then more slowly at a rate of 0.8 °C h^{-1} to 1025 °C then at 0.4 °C h^{-1} to 1000 °C. Finally, the sample was furnace-cooled to a room temperature. The sample was annealed ultimately in a tube furnace in an oxygen atmosphere at 450 °C for 7 d to allow oxygen to penetrate into the single grains and to transform the Gd-123 lattice structure from tetragonal to orthorhombic, which is the target superconducting phase [20].

Measurements and microscopy

The single grain sample was polished flat and its trapped field measured at 77 K. This involved cooling the sample to 77 K in a magnetic field of 1.4 T and removing the applied field over a period of 100 s. A hand-held Hall probe was placed 0.5 mm above the top surface of the sample to determine the maximum trapped magnetic field, with the complete trapped field profile measured subsequently using a rotating array of eighteen Hall probes placed 1.5 mm above the sample surface. The sample was cut along a diameter and through its entire thickness following measurement of the trapped field, as indicated by the two dashed red lines in figure 2(a).

A thin slab was extracted from the single grain sample and then cut further parallel to the c-axis and cleaved along

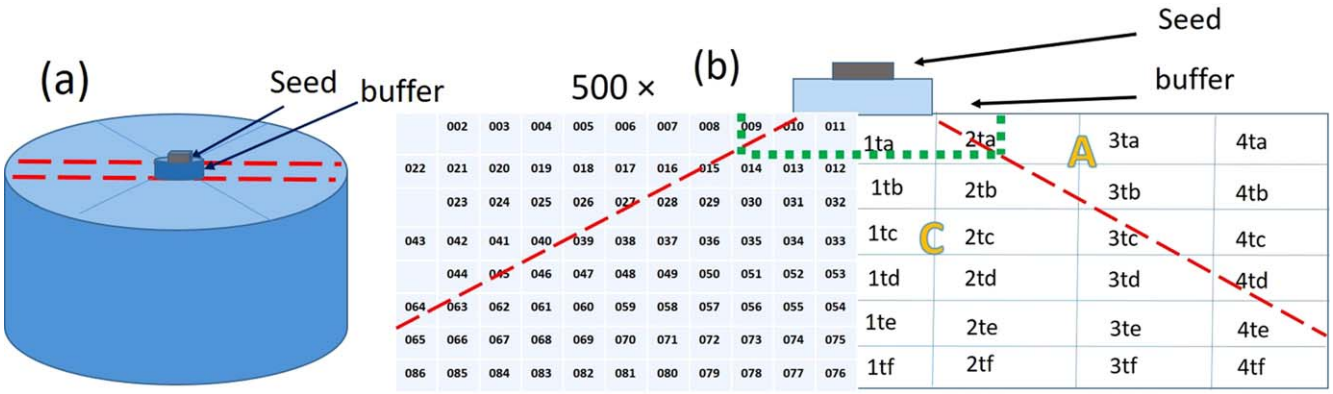

Figure 2. (a) Schematic illustration of a single grain and (b) locations of the sub-specimens used to measure T_c and J_c (right) and the positions of the photographs (left) taken at intervals of 1 mm at a magnification of 500×.

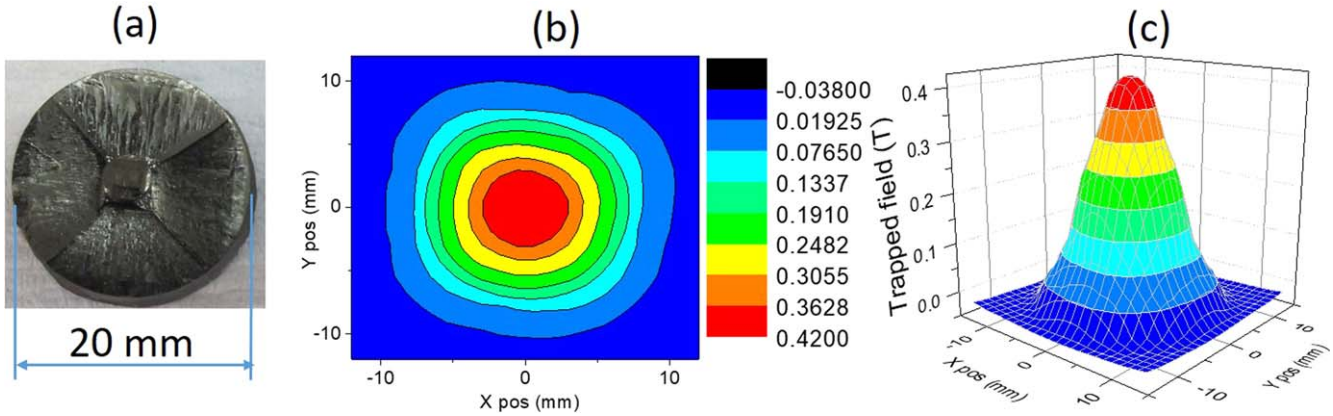

Figure 3. (a) Photograph of the GdBCO single grain (20 mm in diameter). (b) Contour map of the trapped field and (c) trapped field distribution B_z—X–Y measured 1.5 mm above the top surface of the sample.

the *ab* plane into smaller sub-specimens corresponding to locations 1ta, 1tc, etc, each of approximate dimensions $a \times b \times c$ at $1.8 \times 2.8 \times 1.5\ \text{mm}^3$, as shown schematically in figure 2(b). The red dashed line in figure 2(b) indicates the approximate position of the boundary between the A- and the C-growth sectors. T_c and M–H loops of the sub-specimens (24 in total from locations 1ta to 4ta of the first row to 1tf to 4tf of the sixth row) were measured using a superconducting quantum interference device (SQUID). This involved applying a test field of 2×10^{-3} T perpendicular to the *ab* plane of each sub-specimen for the measurement of T_c and using the extended Bean model [21] to calculate J_c using M–H loop data measured for each cuboid, $a \times b \times c$, at 77 K, where a, b, and c are the dimensions of the sample with $a < b$ and c is the specimen dimension in the c direction.

The cross-section of the remaining half sample was polished, and its microstructure examined using an OLYMPUS BX51M optical microscope. In total, 85 images at a magnification of 50× were assembled automatically by LAS BX51M software to reveal the distribution of the pores and cracks over the cross-sectional surface of the sample. Images at higher magnification (500×) were also taken from the edge of the sample to its centre and from the top to the bottom of the half-grain at intervals of 1 mm to examine the distribution of Gd-211 inclusions in order to investigate correlations between local J_c and the associated single grain microstructure. The total count, fraction of area occupied by pores and the average size of the pores of 20 images cropped from figure 4(b) at position exactly equivalent to the positions where J_c were measured were estimated quantitatively using ImageJ software. 20 additional photographs of the cross-section of the sample were taken by SEM at a magnification of 5000× along the *a*- and *c*-axes, starting from the central position and 0.5 mm below the top surface. The area fraction occupied by the Gd-211 inclusions and their average size along the *a*-axis were measured quantitatively using ImageJ software. The single grain was assumed to exhibit a radial symmetry throughout this study.

Results and discussion

Confirmation of single grain growth

Figure 3(a) shows the GdBCO sample used in this study. The four-fold facet lines visible at the top surface and their extension to the bottom of the sample indicate that the sample has grown in the form of a large, single grain. The trapped field profile, B_z—X–Y, is expected to exhibit a single peak if the sample is a single grain, given that B_z is an integral of J_c

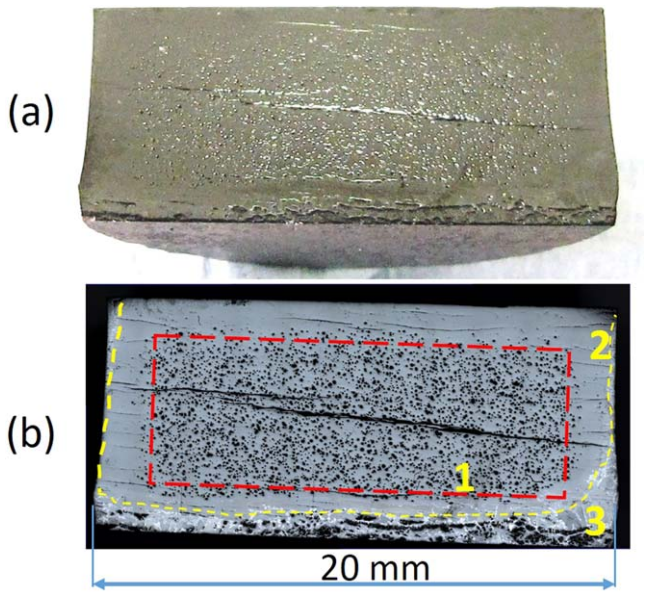

Figure 4. (a) A photograph of the cross-section of the GdBCO single grain 20 mm in diameter and (b) an assembly of 85 photographs taken at 50× magnification of the entire sample cross-section.

over the entire sample volume, so its contour map should consist of concentric, closed lines that follow roughly the shape of the single grain. Figures 3(b) and (c) show the contour map and B_z—X–Y measured by the rotating Hall probe array at a position 1.5 mm above the top surface of the sample. It can been seen further that the sample does, indeed, constitute a single grain from the geometry of the trapped field profile. The peak value measured by the hand probe 0.5 mm above the top surface of the sample is 0.65 T, which is close to the typical value of a GdBCO single grain of this geometry observed previously by our group [22], suggesting that the sample is suitable for analysing the distribution of the local superconducting properties within the body of the single grain.

Microstructure

Low magnification at 50×. Figure 4(a) shows a photograph of the cross-section of the GdBCO single grain. Figure 4(b) shows an assembly of 85 photographs taken using an optical microscope at 50× magnification over the entire cross-section of the sample. Both images are typical of (RE)BCO single grains (where RE = Nd, Sm, Gd, Dy and Y) fabricated in air. Figure 4(b) shows an image of higher resolution than that in figure 4(a), that gives more detail of the microstructure evident on the polished surface, which can be divided into three regions (1–3). There are many pores within region 1 (the red dashed rectangle); the size of the pores is roughly 50 μm on average and it can be seen that the closer to the sample centre, the larger the pore size. A large crack, which was almost certainly caused during the precursor compaction process, crosses the centre of the sample cross-section. Region 2 (between the red dashed line and yellow dashed line), of thickness of 2–3 mm, exhibits significantly reduced porosity and the material appears relatively dense in this region. There are many small, parallel cracks, which are caused during oxygenation as the tetragonal Gd-123 phase transforms to the orthorhombic phase [23]. Region 3 (outside the yellow dashed line) consists of the edges of the sample and where the growth process terminates. It can be seen from the contrast in figure 4(b) that the material in region 3 appears to be different to that of the rest of the sample. The relative proportion of the size of regions 1 and 2 changes from sample to sample, depending on the particular (RE)BCO system, the composition of the precursor powder and the processing route. Published photographs of the cross-sections of YBCO single grains [17,19,24,25] indicate further that all single grains within this system can also be divided, generally, into these three regions. Region 3 is characteristically quite small, of size between 0.5 and 1 mm at the circumference edge and 2 mm at the bottom of the sample in this study, although its thickness may change depending on the substrate material used for the growth of the single grain.

Figure 5(a) shows the total count of pores at 4 positions in all the sample layers (a to e). It can be seen that the total pore count at positions 4 (purple triangles) and within the 'a' layer, which are within the 2nd region in figure 4(b), is low. In addition, there is a sharp increase in porosity in position 2 in all b, c, and d layers and the porosity remains approximately constant right up to the edge of the sample. Figure 5(b) shows the average size (derived from the longest dimension present in a pore) of pores at 4 positions in the different layers. It can be seen that the size of the pores are smaller in the 'a' layer and the pore size increases with increasing proximity to the centre of the sample. The average longest dimension of the pores is 100 μm measured by ImageJ software. Figure 5(c) indicates that the area occupied by the pores can be as high as 25% in the b, c and d layers, which suggests that up to 25% of the cross-section of the single grain sample may not be superconducting.

Gd-211 distribution. Figure 6 shows the microstructure of the GdBCO sample at position 28 (see figure 2(b)). The sample exhibits a typical microstructure expected for a (RE)BCO single grain on this length scale. The continuous background is the superconducting Gd-123 matrix, and the light-in-contrast inclusions are the embedded, non-superconducting Gd-211 particles. The size of the Gd-211 inclusions varies from 1 to 6 μm, with most particles being approximately 2 μm in diameter. There are local areas within the sample microstructure, such as that circled, that are void of Gd-211 particles. It is suggested that these areas were initially pores that became filled by the liquid phase ($Ba_3Cu_5O_8$) at elevated temperature, which later reacted with Gd-211 to form the Gd-123 phase during the growth process [26,27]. A single pore can be seen at the bottom of figure 5, which is expected for an image magnification of 500×, and particularly in photographs taken in the vicinity of the centre of the sample cross-section.

Figure 7 shows a number of photographs taken at a magnification of 500× at different positions within the single grain sample, and from which the distribution of Gd-211 second phase inclusions can be studied. It can be seen that the

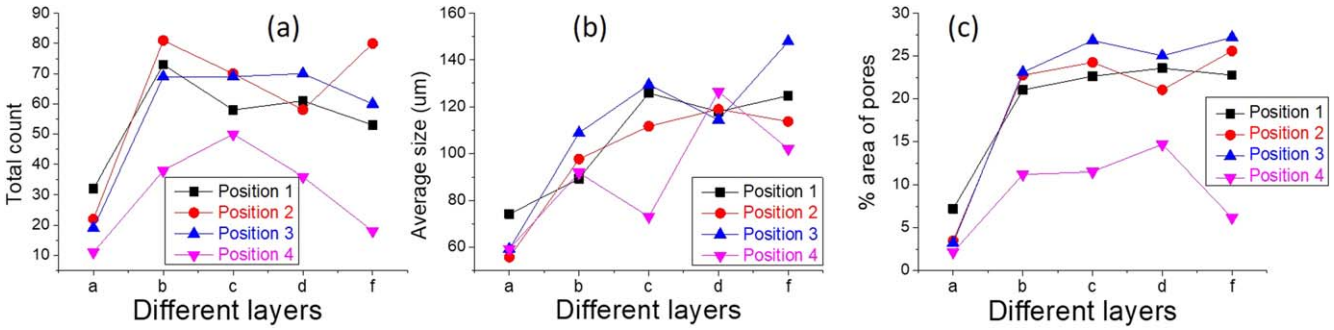

Figure 5. Distribution of the porosity in the cross-section of the GdBCO single grain (a) total count of pores at 4 positions in the different layers, (b) the average size (determined by the longest dimension in a pore) of the pores at 4 positions in different layers and (c) percentage of area occupied by the pores.

Figure 6. A typical photograph at 500× magnification showing the embedded Gd-211 particles in the Gd-123 phase matrix.

number of Gd-211 particles in each image in the a/b growth direction increases and their size becomes slightly smaller with increasing distance (photographs 011, 007 and 002; top row, right to left). This trend can be seen more clearly from the photographs taken at a magnification of 5000× in figure 8. Comparing figures 8(a) and (b), it can be seen that the Gd-211 particles increase in quantity but decrease in average size at a position of 5 mm along *a*-axis. This trend is also indicated by the quantitative analysis of the area fraction occupied by Gd-211 particles and their average size from the SEM images at a magnification of 5000× along the *a*-axis, shown in figure 8(d). Photographs 011, 032, 053 and 075 (right-hand column of figure 7, top to bottom) show the Gd-211 distribution along the *c* growth direction, which follows a similar trend, which also can be seen more clearly from the SEM images taken at a magnification of 5000×, shown in figure 8. Comparing figures 8(a) and (c), it can be seen that the Gd-211 particles increase in quantity but decrease in size with increasing distance along the *c*-axis. The number and size of the Gd-211 inclusions is similar along a given growth front, on the other hand, as indicated by the parallel dashed green lines in figure 2 (apparent by comparing photographs 53 and 49). Many researchers have reported this trend, in the YBCO [28,29], GdBCO, SmBCO and Ag-containing (RE) BCO systems [24, 30–33], and the current study confirms this trend that the amount of embedded Y-211 inclusions along both the a/b and *c* crystallographic growth directions increase under processing conditions of a larger under-cooling temperature, which leads to the formation of a region of low Y-211 concentration in the vicinity of the seed [33].

This distribution of RE-211 content within a single grain is an intrinsic characteristic of the top-seeded melt growth (TSMG) process and can be explained by the so-called push/trap effect [30]. According to pushing/trapping theory, Y-211 particles of size smaller than a critical radius r^* will be pushed by the growth front of the Y-123 single grain. In other words, Y-211 particles of size larger than r^* will be trapped within the growing Y-123 single grain matrix. r^* is also inversely proportional to the growth rate, which is influenced critically by the undercooling and the initial Y-211 composition. In general, the higher undercooling, the lower r^*, which is the case at positions further away from the seed. Although RE-211 particles react with the liquid phase and are therefore not technically inert during the single grain growth process, the push/trap model still provides a very good approximation to the dynamics of the RE-211 particle during the grain growth process.

Comparison of the distribution of Gd-211 within the GdBCO single grain studied here with those reported previously indicates that a different trend is seen in the current sample, due primarily to the use of a buffer beneath the seed. The position under the buffer (1ta) has rather large quantity of RE-211 inclusions, as can be seen from figure 8(d), the blue dots at positions 0, 1 and 2 indicate that Gd-211 can occupy an area as high 20%. This compares to a steep spatial concentration gradient in RE-211 inclusions observed in the vicinity of the seed [33] when a buffer was not used, which can vary typically from 5% to 15% over a distance of 0–2 mm in all (RE)BCO systems investigated to date [24,33]. The use of a buffer and polishing the top surface of the single grain flat for the trapped field measurement resulted in the removal of approximately between 0.5 and 1 mm of material from the top surface of the as-grown sample. As a result, the number of Gd-211 inclusions under the position of the seed at specimen location 1ta is considerably greater than when a buffer is not used, as is apparent from photograph 011 in figure 6. This effect has also

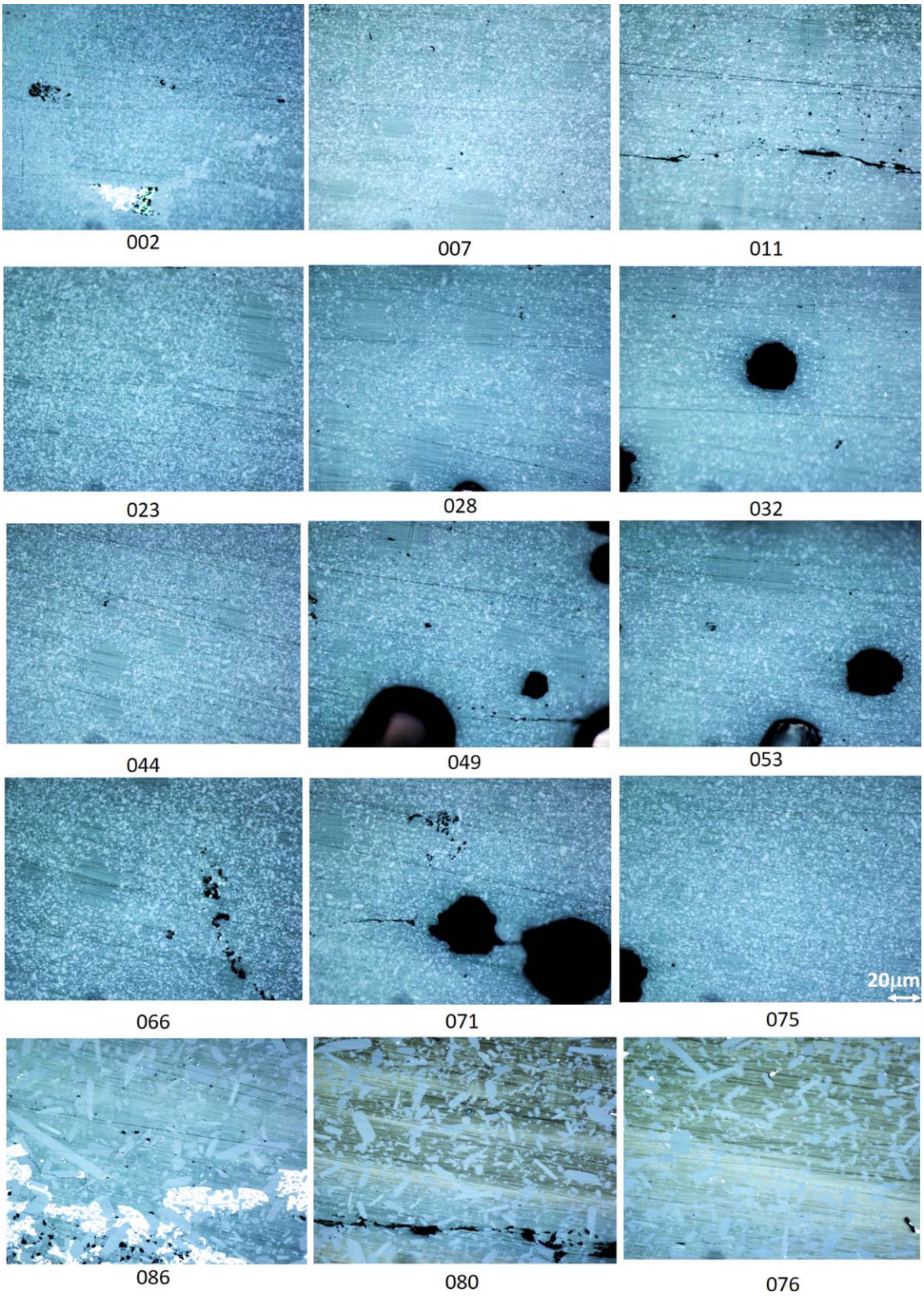

Figure 7. Microstructures of the polished surface from top to bottom and from the centre to the edge of the GdBCO single grain. The position labels are illustrated schematically in figure 2.

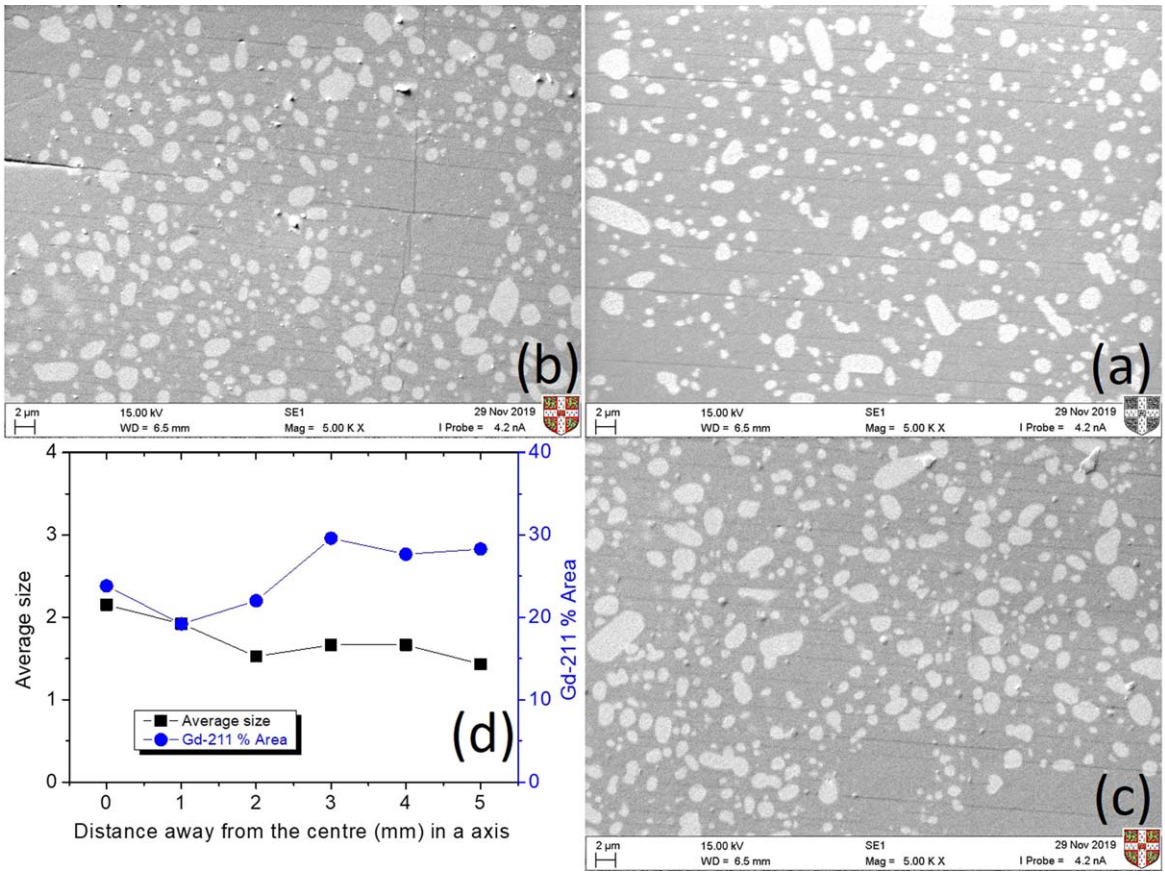

Figure 8. Gd-211 particles at different positions of the cross-section in figure 4. (a) At position 0.5 mm below the top surface at the centre of the single grain, (b) at position 5 mm away from the (a) position along the *a*-axis and (c) at position 5 mm away from the (a) position along the *c*-axis. (d) Distribution of the average size and area occupied by Gd-211 particles along the *a*-axis at the centre of the single grain under the buffer.

been observed in the YBCO system [34] when a buffer was used in the TSMG process. That is to say, the distribution of Gd-211 is relatively uniform in this study, and especially in the vicinity of the seed (or buffer) in the polished top surface of the sample and in the region where microstructure affects significantly the measured trapped field. The region at the centre of the top surface of the sample, and where the RE-211 concentration changes rapidly, has been removed for the GdBCO sample studied here, even though the trend in the size and distribution of the Gd-211 phase is similar as that reported elsewhere.

The edges of the sample (i.e. at the ends of the grain growth process) are shown in figure 7 in the photographs in the left column and 0.5 mm beyond the point at which growth terminates in the 4th and 5th rows of the single grain. It can be seen that there is a large concentration of Gd-211 particles in the regions labelled as 002, 023, 044, 066, 071 and 075 in figure 7, which is anticipated from push/trap theory. Microstructures such as that shown in figure 9 at position 043, which was photographed a further 0.5 mm towards the edge of the sample, show a significant difference from that observed in the bulk of the single grain. The white-in-contrast substance in these micrographs is a Ba-rich phase solidified from the residual liquid phase and impurities, which has been analysed thoroughly in previous research. The microstructures

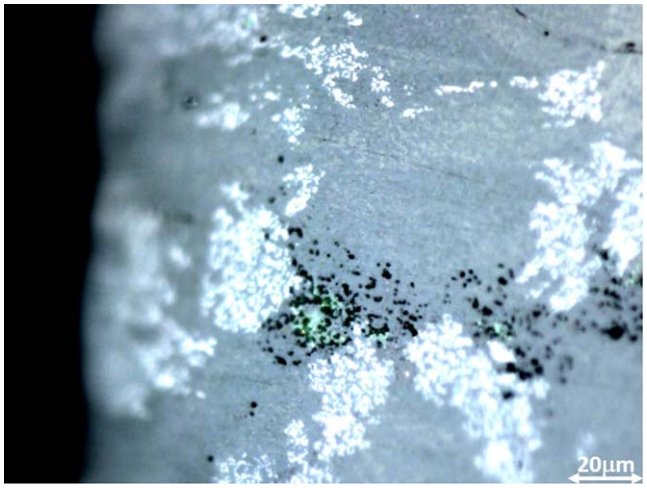

Figure 9. Microstructure at 500× at the edge of the sample, or position 43 in figure 2.

at the very bottom of the sample are shown as 076, 080 and 086. Extremely large inclusions and regions of solidified liquid-rich phase are present in these areas.

In summary, the microstructures at magnifications of 50× and 500× of the polished GdBCO single grain of 20 mm in diameter fabricated by the buffer technique exhibits high

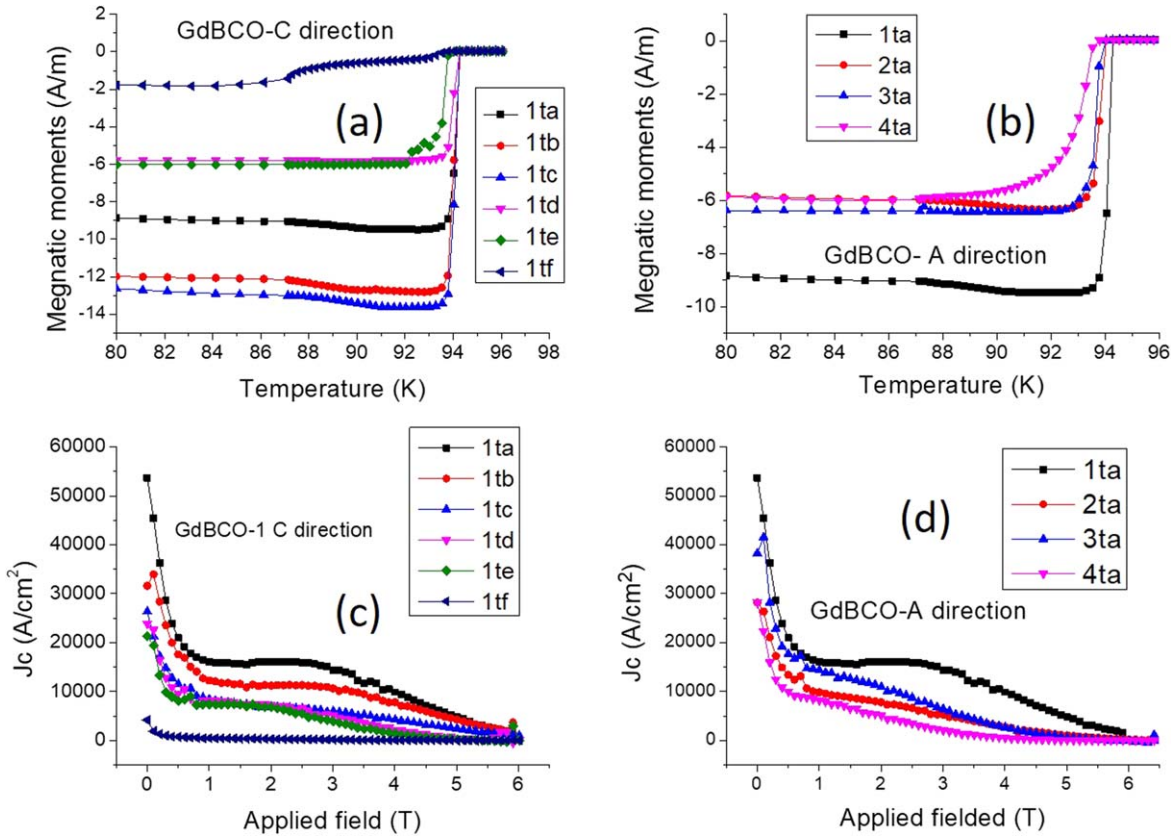

Figure 10. Local T_c and J_c-B for specimens at the centre of the top surface to the edge of the GdBCO single grain along the c and a/b directions.

porosity at the centre of the sample and very low porosity at positions within 2 mm of the edge of the sample. The distribution of Gd-211 particles in the single grain microstructure is described well by push/trap theory, e.g. there are smaller and more Gd-211 at positions further away from the seed along the principal growth directions. However, this change is relatively small when compared to the distribution of RE-211 particles observed in single grains grown by melt processing without a buffer. The edges, either at the circumference or the bottom of the sample, contain a significantly higher concentration of Gd-211 and solidified liquid phase than the rest of the sample.

Superconducting properties: T_c and J_c at 77 K. Figures 10(a) and (b) show the results of the measurements of T_c for specimens located beneath the buffer along the c-axis and across the first-row along the ab plane, respectively. Figures 10(c) and (d) show the equivalent J_c measurements at 77 K for these specimens. The onset values of T_c of the specimens at locations 1ta, 1tb, 1tc and 1td in figure 10(a) are coincident at 93.5 K, and the measured values of ΔT_c are all narrow, which indicates only limited Gd/Ba substitution in these samples and that there is little or no contamination from the seed due to the use of the buffer, as has been reported elsewhere [9,34].

However, the specimens at locations 1te and 1tf have a lower onset T_c and generally exhibit a very broad transition. In particular, the magnetic moment of specimen 1tf (navy curve) is extremely low. This suggests that the volume fraction of superconducting material is reduced compared to that at other locations. Given that all the sub-specimens are of similar size, this can be explained by the location of specimen 1tf at the bottom of the sample, which increases the concentration of liquid-rich phase in its microstructure [25] and, as a result, reduces the volume of the superconducting phase. The onset T_c's at the edges of the single grain, such those observed at positions 4ta in figure 10(b) and 1te in figure 10(a), and at the circumference and bottom of the single grain, are also inferior to those of the other specimens. This is also due to the reduced presence of superconducting phase at these positions, and is associated microstructurally with either the end of the growth process or to the presence of an excess of Gd-211 phase inclusions, as evidenced from the microstructure images in figure 7. This effect from the edges also can be seen in the J_c data in figures 10(c) and (d).

The J_c-B curves in figures 10(c) and (d) were calculated using the extended Bean model. The 'tilt' in the GdBCO M–H loops is due to the paramagnetic nature of Gd, which is superimposed on the superconducting magnetic moment. As a result, the two values of the magnetic moment derived from the M–H loop to obtain ΔM (for increasing and decreasing field, respectively) are not symmetric about the x-axis (field is the x-axis), which leads $J_c(0)$ to be lower than $J_c(0.1)$ in some cases, such as the J_c-B curve for specimens at locations 1tb and 3ta in figures 10(c) and (d). It was expected that specimen 1tf would exhibit low J_c, given its broad T_c and poor

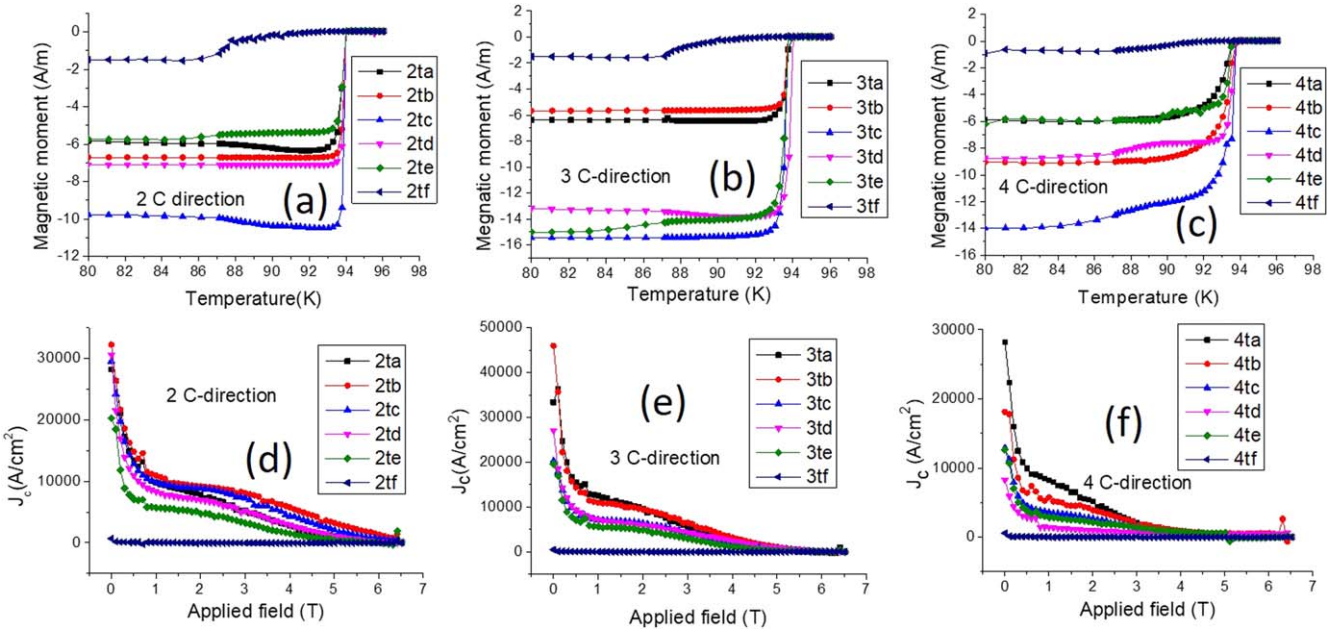

Figure 11. Local T_c and J_c-B of the complete half cross-section of the GdBCO single grain. (a)–(c) Measurements of T_c at positions 2, 3 and 4 along the sample c direction. (d)–(f) J_c-B curves at positions 2, 3, and 4 positions along the c direction.

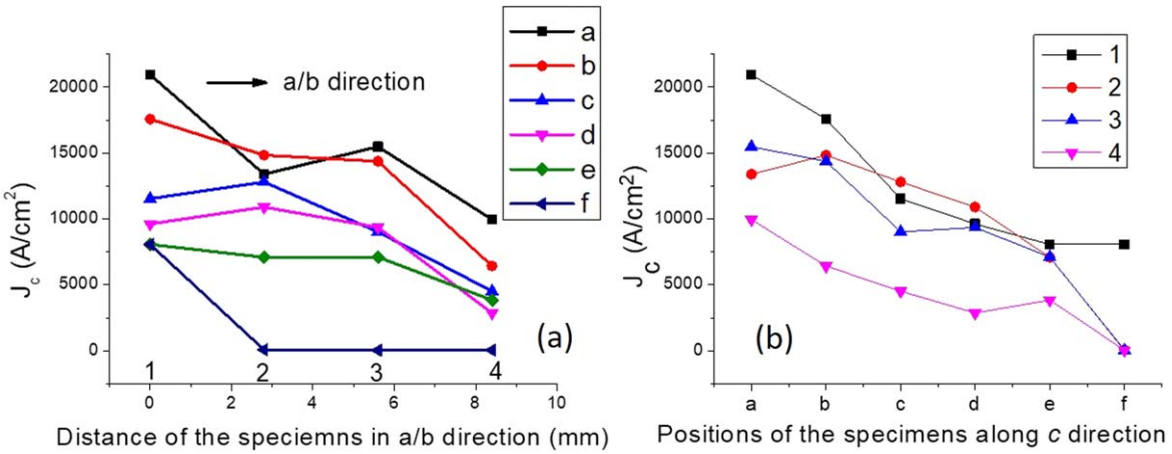

Figure 12. Local T_c and J_c measured at an applied field 0.5 T from the centre of the top surface of the single grain to the edge along (a) the a/b direction and (b) the c direction.

superconducting properties. The J_c-B curves along the c direction in figure 10(c), however, show that sub-specimens 1ta and 1tb have consistently the highest J_c at all applied fields and exhibits the 'peak' effect [35] (in which J_c increases under the influence of an externally applied field, up to a threshold value), whereas other specimens, such as 1tc, 1td and 1te, exhibit similar J_c-B curves at all applied fields and do not show the peak effect.

Figure 11 shows the T_c and J_c-B curves of the remaining specimens in the single grain cross-section. The onset of T_c is the same at 93.5 K, and ΔT_c is relatively narrow except the edge of the parent sample in row f and column four. Similarly, J_c decreases from top to bottom of the single grain for specimens 2ta to 2tf in figure 11(d), 3ta to 3tf in figure 11(e) and 4ta to 4te in figure 11(f). Significantly, the J_c data shown in figure 11(f) are lower since these specimens are at the edge of the single grain. In general the J_c-B curves are almost monotonic and hence do not intersect with each other. J_c at 0.5 T is replotted with respect to location in figure 12.

It can be seen clearly from figure 12(b) that J_c decreases along the c direction of the single grain. However, the trend along the a/b direction is not as apparent as that along c, with the measured values of J_c in layers d and e being almost constant, except at the edges of the sample, where J_c of specimens in column four are low. The values of J_c in layers a, b and c along the a/b direction decrease from the centre to the edge of the sample relative to J_c values observed at positions 4. J_c at the specimen position immediately beneath the buffer is the highest, which is not the same as observed previously in an early investigation [6].

It is observed generally that J_c is dependent on the volume fraction of RE-211 in the single grain microstructure

[36]. However, the previous research only suggests when the weight percentage of RE-211 is not changed, the resulted smaller and more numerous inclusions of RE-211 increase local J_c, therefore trapped field [36–39]. The distribution of Gd-211 particles in this study, indeed, shows an increase in volume fraction with very little variation along both principal growth directions, although there is a small variation along the c direction. However, this is not sufficient to cause the observed trend in J_c. It can be seen from figure 12(a) that values of the J_c in layers a and b layers (black and red) are a factor of two larger than those in layers c, d and e. Although, theoretically, J_c varies in proportion to the number of pinning centres, including stacking flaws, twins and Gd-211-related pinning sites, the distribution, and therefore contribution to trapped field, of these pinning centres within the bulk microstructure can be very complicated. The difference between layers a, b layers and layers c, d, e is that the latter appear to contain a greater number of large, non-superconducting defects and large pores that cannot work effectively as flux pinning centres towards the centre of layers b, c, d and e. By comparing the quantitative distribution of the porosity shown in figure 5 and the quantitative distribution of Gd-211 in figure 8(d) with figure 12(b), it is likely that the existence of these large non-superconducting pores contributes significantly to the lower observed values of J_c in layers c, d, e. The negative contribution of this microstructural feature to J_c is more pronounced than the positive contribution from enhanced flux pinning by the Gd-211 phase in this sample. This also explains why J_c declines rather rapidly along the c-axis of the single grain due to the rapid change from a dense to a more porous material, and, finally, to a solidified non-superconducting phase from specimen positions 1ta to 1te. The highest value of $J_c(0.5)$ (specimen position 1ta) in the first row of the sample is 3 times the value of the lowest positioned specimen $J_c(0.5)$, even if the specimen at the edge (1tf) is discounted. The effect of microstructure (mainly porosity) on the value of local J_c can also explain its observed trend along the a/b direction (figure 12(a)). The variation in J_c at the first, second and third positions in a particular layer is less (other than at specimen position 1ta) due to the similar observed levels of porosity up to the edge of the single grain (specimen position 4). The J_c at specimen position 1ta is relatively high for other reasons, such as the integrity and alignment of the lattice to the orientation of the single crystal seed in the vicinity of the seed/buffer [13]. In summary, by comparing figures 5(b) and 12(b) in which the x-axes are the same, it can be seen clearly that the porosity is low and the values of J_c high within the a layers, whereas for the remaining layers (b, c, d and e), the porosity is high and the values of J_c low. It is not possible, therefore, for the distribution of Gd-211 particles to influence significantly the distribution of J_c in layers b–e, given the non-superconducting nature of pores, which is a more dominant influence on J_c.

It can be seen further that low J_c occurs consistently in specimens in regions at the end of the growth process, which constitute the edges of the circumference of the single grain (specimens 4ta, 4tb, 4ta and 4td) and the bottom layer (f). This is consistent with the observed low T_c for these specimens that also exhibit a very broad transition due to the presence of both a relatively large number of Gd-211 phase inclusions, solidified, non-superconducting liquid phase and impurities, which reduce J_c much more severely than the presence of pores in an otherwise strongly superconducting phase matrix. In addition, the effect at the edges of the sample is more pronounced with increasing distance along the growth direction, as indicated by specimens 4te and 4tf, which exhibit the worst properties of T_c and J_c in the entire sample.

The observed trend in the distribution of J_c is consistent with the results of a previous study [6] (figures 3 and 4 therein) allowing for contamination in the region beneath the seed, which reduces T_c. J_c in the middle layer of the single grain is also higher than that observed in the bottom layer [6]. However, the previous study of the distribution of J_c did not measure the properties of specimens at the extreme edges of the sample, such as at locations 4, and the sample was not melt processed with a buffer. J_c in the a/b direction in the present study is relatively constant, although it does fluctuate within a range of approximately ± 1500 A cm^{-2} in all layers (a, b, c, d and e) of the single grain (apart from J_c at 1ta) if the J_c values at positions 4 are not taken into account. The same trend in J_c along the c growth direction has also been reported for the YBCO system [40] processed in air by TSMG using a buffer. It is clear, therefore, that J_c decreases rather rapidly from top to bottom of the single grain along the c direction. On the other hand, J_c is relatively constant within a given layer in the a/b direction and there is no clear correlation between the distribution of RE-211 and the local J_c within one single grain.

Conclusions

Systematic examination of the cross-section of a GdBCO single grain fabricated by buffer-aid TSMG has shown that the sample can be considered to consist of three regions. The first region, at the centre of the grain, contains many pores, the second region, closer to the edges, is denser and the third region, at the very edges, is composed generally of a concentration of RE-211 particles and solidified liquid phase with embed impurities.

The number of Gd-211 inclusions increases gradually along both principal growth directions and their size becomes smaller, as reported previously for the GdBCO system. The presence of porosity in the single grain microstructure appears not to influence the distribution of the Gd-211 particles. However, the observed concentration gradient of the Gd-211 inclusions is less steep for the GdBCO sample investigated in this study, and especially in the region of the seed (around 1.5 mm in diameter). This is attributed to the use of a buffer and the polished surface of sample, which increases the effective concentration of Gd-211 particles at the centre of the top surface of the single grain.

J_c decreases along the c-growth direction from top to bottom of the single grain, but varies much less along the a/b direction, ignoring the edges of the sample. The same

distribution has been reported for YBCO single grains, for which RE/Ba substitution effects are not an issue (i.e. the onset T_c is high and ΔT_c is narrow for the entire sample away from the sample edges).

The effect that the edges of the sample exhibit the lowest and the broadest T_c hence lowest J_c has been demonstrated clearly in this study, and is due to the concentration of Gd-211 particles and presence of solidified liquid phase and impurities in these regions.

In summary, this study suggests that the observed trend in J_c at different positions in the single grain GdBCO sample prepared using a buffer and additional liquid phase is significantly different to that observed for the size and concentration of RE-211 particles. In particular, there is no clear correlation between the distribution of RE-211 inclusions and local J_c within the single GdBCO grain. The porosity of the sample, on the other hand, is a much more dominant factor in determining the distribution of J_c than Gd-211 particles. The highest quality material occurs is at the centre of the top surface of the sample, whereas porosity at the centre and poor superconductivity at the edges of the single grain are responsible for the rapid decrease of the J_c along the c-axis growth direction. The importance of porosity in controlling local critical current density suggests that process refinement aimed at reducing porosity may help improve the uniformity of J_c within a single GdBCO grain.

Acknowledgments

The authors acknowledge the financial support from the Engineering and Physical Sciences Research Council EP/P00962X/1. Additional data related to this publication are available at the University of Cambridge data repository (https://doi.org/10.17863/CAM.44165)

ORCID iDs

Yunhua Shi https://orcid.org/0000-0003-4240-5543
John H Durrell https://orcid.org/0000-0003-0712-3102

References

[1] Todt V R, Zhang X F, Miller D J, St. Louis-Weber M and Dravid V P 1996 Controlled growth of bulk bicrystals and the investigation of microstructure-property relations of $YBa_2Cu_3O_x$ grain boundaries *Appl. Phys. Lett.* **69** 3746–8
[2] Dimos D, Chaudhari P and Mannhart J 1990 Superconducting transport properties of grain boundaries in $YBa_2Cu_3O_7$ bicrystals *Phys. Rev.* B **41** 4038–49
[3] Salama K, Selvamanickam V, Gao L and Sun K 1989 High current density in bulk $YBa_2Cu_3O_x$ superconductor *Appl. Phys. Lett.* **54** 2352–4
[4] Krabbes G *et al* 2000 Zn doping of $YBa_2Cu_3O_7$ in melt textured materials: peak effect and high trapped fields *Physica* C **330** 181–90
[5] Shlyk L, Nenkov K, Krabbes G and Fuchs G 2005 Melt-processed YBCO with Pt or Ce additions: comparison of pinning behavior *Physica* C **423** 22–8
[6] Dewhurst C D, Wai L and Cardwell D A 1997 Distribution of critical current density in large $YBa_2Cu_3O_{7-\delta}$ grains fabricated using seeded peritectic solidification *IEEE Trans. Appl. Supercond.* **7** 1925–8
[7] Iida K, Babu N H, Shi Y and Cardwell D A 2005 Seeded infiltration and growth of large, single domain Y–Ba–Cu–O bulk superconductors with very high critical current densities *Supercond. Sci. Technol.* **18** 1421
[8] Lo W, Cardwell D A, Dewhurst C D, Leung H T, Chow J C L and Shi Y H 1997 Controlled processing and properties of large Pt-doped Y–Ba–Cu–O pseudocrystals for electromagnetic applications *J. Mater. Res.* **12** 2889–900
[9] Li T Y *et al* 2010 Growth and superconductivity of REBCO bulk processed by a seed/buffer layer/precursor construction *Supercond. Sci. Technol.* **23** 125002
[10] Difan Z *et al* 2012 MgO buffer-layer-induced texture growth of RE–Ba–Cu–O bulk *Supercond. Sci. Technol.* **25** 025022
[11] Lee J H *et al* 2011 A buffer bridge process for growing multiple $YBa_2Cu_3O_{7-y}$ grains from one top seed *Supercond. Sci. Technol.* **24** 055019
[12] Shi Y H, Dennis A R and Cardwell D A 2015 A new seeding technique for the reliable fabrication of large, SmBCO single grains containing silver using top seeded melt growth *Supercond. Sci. Technol.* **28** 035014
[13] Devendra Kumar N, Shi Y, Zhai W, Dennis A R, Durrell J H and Cardwell D A 2015 Buffer pellets for high-yield, top-seeded melt growth of large grain Y–Ba–Cu–O superconductors *Cryst. Growth Des.* **15** 1472–80
[14] Kim C J, Lee J H, Park S D, Jun B H, Han S C and Han Y H 2010 Y_2BaCuO_5 buffer block as a diffusion barrier for samarium in top seeded melt growth processed $YBa_2Cu_3O_{7-y}$ superconductors using a $SmBa_2Cu_3O_7$ −dseed *Supercond. Sci. Technol.* **24** 015008
[15] Cardwell D A 1998 Processing and properties of large grain (RE)BCO *Mater. Sci. Eng.* B **53** 1–10
[16] Shi Y, Babu N H and Cardwell D A 2005 Development of a generic seed crystal for the fabrication of large grain (RE)–Ba–Cu–O bulk superconductors *Supercond. Sci. Technol.* **18** L13
[17] Yunhua S, Devendra Kumar N, Wen Z, John H D, Anthony R D and David A C 2016 The use of buffer pellets to pseudo hot seed (RE)–Ba–Cu–O–(Ag) single grain bulk superconductors *Supercond. Sci. Technol.* **29** 015010
[18] Shi Y, Namburi D K, Wang M, Durrell J, Dennis A and Cardwell D 2015 A reliable method for recycling (RE)–Ba–Cu–O (RE: Sm, Gd, Y) bulk superconductors *J. Am. Ceram. Soc.* **98** 2760–6
[19] Namburi D K, Shi Y, Palmer K G, Dennis A R, Durrell J H and Cardwell D A 2016 An improved top seeded infiltration growth method for the fabrication of Y–Ba–Cu–O bulk superconductors *J. Eur. Ceram. Soc.* **36** 615–24
[20] Hatano T, Matsushita A, Nakamura K, Sakka Y, Matsumoto T and Ogawa K 1987 Superconducting and transport properties of B–Y–Cu–O compounds -orthorhombic and tetragonal phases *Japan. J. Appl. Phys.* **26** L721–3
[21] Chen D X and Goldfarb R B 1989 Kim model for magnetization of type-II superconductors *J. Appl. Phys.* **66** 2489–500
[22] Cardwell D A, Shi Y and Namburi D K 2019 Reliable single grain growth of (RE)BCO bulk superconductors with enhanced superconducting properties *Supercond. Sci. Technol.* **33** 024004
[23] Diko P and Krabbes G 2002 Macro-cracking in melt-grown YBaCuO superconductor induced by surface oxygenation *Supercond. Sci. Technol.* **16** 90–3

[24] Congreve J V J, Shi Y H, Dennis A R, Durrell J H and Cardwell D A 2016 Microstructure and composition of primary and recycled single grains of YBCO, GdBCO-Ag, and SmBCO-Ag bulk superconductors *J. Am. Ceram. Soc.* **99** 3111–9

[25] Congreve J V J, Shi Y, Dennis A R, Durrell J H and Cardwell D A 2016 Improvements in the processing of large grain, bulk Y–Ba–Cu–O superconductors via the use of additional liquid phase *Supercond. Sci. Technol.* **30** 015017

[26] Murakami M 1992 *Melt Processed High Temperature Superconductors* (Singapore: World Scientific)

[27] Kim C-J, Kim K-B, Won D-Y and Hong G-W 1994 Entrapment of Ba–Cu–O liquid phase during growth of a $Y_1Ba_2Cu_3O_{7-y}$ domain *Physica* C **228** 351–8

[28] Chow J C L, Lo W, Leung H T, Dewhurst C D and Cardwell D A 1998 Processing, Y_2BaCuO_5 distribution and critical current density in large grain Pt-doped YBCO *Mater. Sci. Eng.* B **53** 79–85

[29] Diko P, Gawalek W, Habisreuther T, Klupsch T and Görnert P 1995 Influence of Y_2BaCuO_5 particles on the microstructure of $YBa_2Cu_3O_{7-x}$ (123)-Y_2BaCuO_5 (211) melt-textured superconductors *Phys. Rev.* B **52** 13658–64

[30] Endo A, Chauhan H S, Egi T and Shiohara Y 1996 Macrosegregation of $Y_2Ba_1Cu_1O_5$ particles in $Y_1Ba_2Cu_3O_{7-\delta}$ crystals grown by an undercooling method *J. Mater. Res.* **11** 795–803

[31] Izumi T, Nakamura Y and Shiohara Y 1992 Diffusion solidification model on Y-system superconductors *J. Mater. Res.* **7** 1621–8

[32] Izumi T, Nakamura Y and Shiohara Y 1993 Crystal growth mechanism of $YBa_2Cu_3O_y$ superconductors with peritectic reaction *J. Cryst. Growth* **128** 757–61

[33] Zhai W, Shi Y, Durrell J H, Dennis A R and Cardwell D A 2014 The influence of Y-211 content on the growth rate and Y-211 distribution in Y–Ba–Cu–O single grains fabricated by top seeded melt growth *Cryst. Growth Des.* **14** 6367–75

[34] Shi Y, Kumar Namburi D, Zhao W, Durrell J H, Dennis A R and Cardwell D A 2015 The use of buffer pellets to pseudo hot seed (RE)–Ba–Cu–O–(Ag) single grain bulk superconductors *Supercond. Sci. Technol.* **29** 015010

[35] Murakami M *et al* 1994 Flux pinning in melt-grown $NdBa_2Cu_3Oy$ and $SmBa_2Cu_3Oy$ superconductors *Japan. J. Appl. Phys.* **33** L715–7

[36] Nariki S, Sakai N, Murakami M and Hirabayashi I 2004 High critical current density in RE–Ba–Cu–O bulk superconductors with very fine RE_2BaCuO_5 particles *Physica* C **412–414** 557–65

[37] Babu N H, Withnell T D, Iida K and Cardwell D A 2007 Strongly coupled artificial bulk HTS grain boundaries with high critical current densities *IEEE Trans. Appl. Supercond.* **17** 2949–52

[38] Iida K, Babu N H, Reddy E S, Shi Y H and Cardwell D A 2005 The effect of nano-size ZrO_2 powder addition on the microstructure and superconducting properties of single-domain Y–Ba–Cu–O bulk superconductors *Supercond. Sci. Technol.* **18** 249

[39] Shi Y *et al* 2012 Synthesis of $YBa_2Cu_3O_{7-\delta}$ and Y_2BaCuO_5 nanocrystalline powders for YBCO superconductors using carbon nanotube templates *ACS Nano* **6** 5395–403

[40] Shewale S 2017 Fabricating Single grain Superconductors from Raw Oxides *Report* of IIB project Engineering Department, University of Cambridge